Organic Electronics 12 (2011) 1755–1762

Contents lists available at ScienceDirect

Organic Electronics

journal homepage: www.elsevier.com/locate/orgel

Molecular-weight-dependent nanoscale morphology in silole-containing cyclopentadithiophene polymer and fullerene derivative blends

Jen-Hsien Huang [a], Fang-Chung Chen [b], Cheng-Lun Chen [c], Annie Tzuyu Huang [a], Yu-Sheng Hsiao [b], Chin-Min Teng [c], Feng-Wen Yen [c], Pelin Chen [a], Chih-Wei Chu [a,b,*]

[a] Research Center for Applied Sciences, Academia Sinica, Taipei, Taiwan
[b] Department of Photonics, National Chiao Tung University, Hsinchu, Taiwan
[c] Luminescence Technology Corporation, Hsinchu, Taiwan

ARTICLE INFO

Article history:
Received 19 May 2011
Received in revised form 13 June 2011
Accepted 19 June 2011

Keywords:
Solar cells
Bulk heterojunction
Molecular weight
Morphology
Phase separation
Exciton lifetime

ABSTRACT

We have investigated the effect of polymer molecular weight (MW) on the morphology and efficiency of bulk heterojunction (BHJ) solar cells comprised of poly[(4,4′-bis(2-ethylhexyl)dithieno[3,2-b:2′,3′-d]silole)-2,6-diyl-*alt*-(5,5′-thienyl-4,4′-dihexyl-2,2′-bithiazole)-2,6-diyl] (Si-PCPDTTBT) and [6,6]-phenyl C_{61} butyric acid methyl ester (PCBM). Striking morphological changes are observed in BHJ films upon the change of the polymer MW. Atomic force microscopy and transmission electron microscopy studies suggest that high MW polymer generated high degree of phase separation, leading to formation of an interpenetrating network for carrier transport. The X-ray diffraction investigation indicated that increased π–π stacking in Si-PCPDTTBT with increasing polymer MWs results in an increase in hole mobility of Si-PCPDTTBT and electron mobility of PCBM as well as the red shift absorption spectrum in BHJ films. The solar cells based on PCBM with high-MW Si-PCPDTTBT deliver power conversion efficiencies of 3.33%.

© 2011 Elsevier B.V. All rights reserved.

1. Introduction

As the need for renewable energy sources becomes more and more urgent, the study of photovoltaic energy conversion is attracting increasing interest, and state-of-the-art organic photovoltaic cells (OPVs) have gained more and more attention from academia and industry because of their substantial future prospects such as low-cost, flexible, and large area applications. Since the invention of the first bulk heterojunction (BHJ) structure through the blending of conjugated polymers as electron donors and fullerene derivatives as electron acceptors [1], the power conversion efficiency of organic solar cells have been dramatically enhanced because excitons can be generated within diffusion length. Although the BHJ provides a large interface for exciton separation, the efficiency is still limited by the carrier recombination in isolated pockets, low carrier mobility and the space charge effect due to unfavorable morphology in such structure. To solve above problems, many approaches, such as thermal annealing [2–4], solvent annealing [5–7], processing additives [8–10] and interface engineering [11–25] have been devoted to form bicontinuous nanophase morphology to increase exciton dissociation and carrier transport. Besides improving through process engineering, the development of film morphology also relates to continuous improvements in the polymer itself, such as solubility [26], average MW [27–29], and chemical architectures [30]. Therefore, understanding the determining factors of the film morphology is a key to improve the performance of BHJ solar cells.

Compared with small molecules, photovoltaic devices fabricated from polymers are much incontrollable by virtue of the variation from MW and polydispersity index. In order to obtain the cell performance with small variation, precisely controlling the polymer MW is crucial

* Corresponding author at: Research Center for Applied Sciences, Academia Sinica, Taipei, Taiwan. Tel.: +886 2 27898000x70; fax: +886 2 27826680.
E-mail address: gchu@gate.sinica.edu.tw (C.-W. Chu).

1566-1199/$ - see front matter © 2011 Elsevier B.V. All rights reserved.
doi:10.1016/j.orgel.2011.06.017

for device optimization. More importantly many researches have been reported that the film morphology and carrier mobility are significantly affected by the MW of poly(3-hexylthiophene) (P3HT) [31–33]. For example, Heeger et al. found that the optimum annealing temperature for bulk heterojunction material is related to the MW of P3HT [31]. The devices made of higher MW P3HT exhibits higher performance because of the persistence conjugation length of polymer chain and the proper interconnections within bicontinuous network. However, P3HT is not the ideal polymer due to its relatively large bandgap. It is essential to obtain low band gap material so light-harvesting abilities of polymers can be enhanced to improve BHJ device efficiencies. One successful approach to low bandgap materials involved donor–acceptor (D–A) copolymers, in which electron-rich units and electron-deficient moieties are integrated into a single conjugated polymeric system. Furthermore, replacing the bridge carbon atom in cyclopentadithiophene (CPDT)-based copolymers with a silicon atom has been shown to be an efficient way to improve solar cell performance [34–36]. The silole-based polymer is found to feature better crystallinity, lower bimolecular recombination, favorable morphology and higher carrier mobility compared with its carbon counterpart. While D–A copolymers have been developed for efficient BHJ solar cells, the differences in their MW and their impact on the film morphology and the opto-electronic properties have not been thoroughly addressed. In this article, we investigated the influence of MW on various optical and physico-chemical properties of Si-PCPDTTBT:PCBM films. We have also correlated the morphology and exciton lifetime distribution for the Si-PCPDTTBT:PCBM films with various MWs. Finally, the photovoltaic performances of the devices based on the hybrids with different MWs are also presented.

2. Experimental

2.1. Material

Monomers M1 and M2 were synthesized according to a reported procedure [36], and the characterization is described as follows. The synthetic route of copolymer Si-PCPDTTBT is shown in Schemes 1, and the procedure is described as follows:

M1. Yield: 65%. ^{1}H NMR: δ 7.03 (d, 2H), 6.92 (d, 2H), 2.86 (t, 4H), 1.72 (m, 4H), 1.40–1.15 (m, 12H), 0.86 (t, 6H). EI-MS: m/z 656. M2. Yield: 92%. ^{1}H NMR: δ 7.06 (s, 2H), 1.68 (m, 2H), 1.4–1.13 (m, 16H), 0.90 (t, 6H), 0.83 (t, 6H), 0.74 (m, 4H), 0.32 (s, 18H).

2.2. General procedure of polymerzation

A solution of M1 (2.00 g, 2.68 mmol) and M2 (1.70 g, 2.68 mmol) in toluene (40 mL) was purged with Ar for 10 min and then $Pd(PPh_3)_4$ (0.150 g, 0.134 mmol) and triphenylphosphine (0.21 g, 0.80 mmol) were added. After purging with Ar for 20 min, the mixture was heated under reflux in an oil bath set at 110 °C under an Ar atmosphere. The mixture was cooled to room temperature, MeOH (100 mL) was added, and the precipitated polymer was filtered out. After Soxhlet extraction with MeOH, hexane, and $CHCl_3$, the polymer was recovered from the $CHCl_3$ phase through reprecipitation with MeOH and then dried under vacuum for 1 day. The MW of polymer was controlled by changing the reaction time, which was monitored by GPC. In this study, Si-PCPDTTBT with four different MWs was synthesized. The reaction times were 6, 10, 24, and 48 h, respectively. The detail information of the MWs for the as-prepared polymers are shown in Table 1.

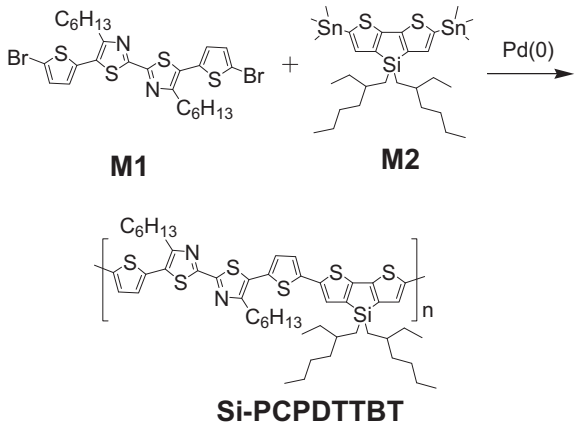

Scheme 1. Synthetic Route of Si-PCPDTTBT Copolymer.

2.3. Device fabrication

The polymer solar cells are consisted of a layer of the Si-PCPDTTBT/PCBM blend thin film sandwiched between a transparent anode (ITO) and a metal cathode. Prior to device fabrication, the ITO glasses (1.5×1.5 cm^2) were cleaned ultrasonically in detergent, deionized water, acetone, and isopropyl alcohol. After routine solvent cleaning, the substrates were treated with UV ozone for 15 min. The modified ITO surface was then obtained by spin-coating a layer of PEDOT:PSS (ca. 30 nm). Subsequently, the active layer, Si-PCPDTTBT/PCBM (1:2 w/w), was spin-coated from DCB onto the PEDOT:PSS-modified ITO surface. Finally, layers of Ca (30 nm) and Al (100 nm) were thermally evaporated under vacuum (pressure: $<6 \times 10^{-6}$ torr) through a shadow mask. The active area of the device was 0.12 cm^2. In the hole-only devices, Ca was replaced with MoO_3

Table 1
Summary of the MWs, polydispersities (PDI) and yields of Si-PCPDTTBT samples in this study.

Sample of Si-PCPDTTBT	Reaction Time (hours)	M_n[a] (kg/mol)	M_w[a] (kg/mol)	PDI	Yield (%)
Low MW	6	6.3	12.2	1.93	61
Medium MW	10	12.7	15.7	1.23	55
	24	22.9	27.3	1.19	57
High MW	48	33.6	38.9	1.15	56

[a] Molecular weights and polydispersity were measured by GPC, using THF as an eluent, polystyrene as a standard. *M*n, number average molecular weight. *M*w, weight average molecular weight.

Table 2
Summary of the transition temperature of Si-PCPDTTBT with various MWs.

Sample of Si-PCPDTTBT	T_g[a] (°C)	T_m[a] (°C)	T_c[a] (°C)	T_d[b] (°C)
Low MW	163	239	n.d.[c]	375
Medium MW	167	245	n.d.[c]	390
	165	251	227	429
High MW	166	253	234	430

[a] The T_g, T_m and T_c were measured by DSC at a heating rate of 10 °C/min.
[b] Temperature (°C) at 5% weight loss measured by TGA at a heating rate of 10 °C/min under nitrogen.
[c] No noticeable transition temperature was observed.

because its higher work function (Φ = 5.3 eV) provided a better hole injection contact for Si-PCPDTTBT/PCBM. A layer of 20 nm thick MoO_3 was thermally evaporated and then it was capped with a layer of Al (50 nm). For the electron-only devices, the PEDOT:PSS layer was replaced with $CsCO_3$ (Φ = 2.9 eV), which is an efficient electron injection layer. This layer of Cs_2CO_3 was thermally evaporated to a thickness of 2 nm. The active layers were then annealed at 130 °C for 20 min to provide the final hole- and electron-only devices.

2.4. Characteriaztion

The cell performance was tested under simulated AM 1.5 G irradiation at 100 mW cm^{-2} using a Xe lamp-based solar simulator (Thermal Oriel 1000 W). The light intensity was calibrated using a mono-silicon photodiode equipped with a Hamamatsu KG-5 color filter. The whole measurement process was performed at room temperature in a glove box filled with N_2. The absorption spectra were obtained from Jasco-V-670 UV-visible spectrophotometer. X-ray diffraction (XRD) studies were performed by Philips X'Pert/MPD. For the fluorescence measurements, the samples were excited with light (wavelength: 470 nm) from a picosecond laser (LDH-P-C-470, PicoQuant); the fluorescence lifetime signal was measured using time-correlated single photon counting (TCSPC). To map the lifetime images, the samples were scanned using an Olympus FV300 confocal optical microscope equipped with a PicoQuant PDM single photon avalanche diode detector and a PicoQuant PicoHarp 300 USB interface for TCSPC. The fluorescence signal was improved using an edge filter (REF-473.0-25, CVI). The acquisition time for each lifetime image (pixel size: 512 × 512) was 20 min. The surface morphologies of the polymer films were investigated using an atomic force microscope (Digital Instrument NS 3a controller equipped with a D3100 stage). The EQE action spectra were obtained under short-circuit conditions. The light source was a 450-W Xe lamp (Oriel Instrument, model 6266) equipped with a water-based IR filter (Oriel Instrument, model 6123NS). The light output from the monochromator (Oriel Instrument, model 74100) was focused onto the photovoltaic cell under test.

3. Results and discussion

Scheme 1 shows the chemical structure and the synthetic route of Si-PCPDTTBT. On the basis of the electron donor–acceptor concept, the strong electron–accepting

Table 3
List of electron and hole mobility of devices based on Si-PCPDTTBT:PCBM with various MWs.

Sample	Low MW	Medium MW		High MW
	6.3	12.7	22.9	33.6
μ_e (m^2 V^{-1} s^{-1})	9.7×10^{-8}	1.1×10^{-7}	1.5×10^{-7}	2.7×10^{-7}
μ_h (m^2 V^{-1} s^{-1})	4.5×10^{-8}	6.4×10^{-8}	9.6×10^{-8}	1.9×10^{-7}
μ_e/μ_h	2.2	1.7	1.6	1.4

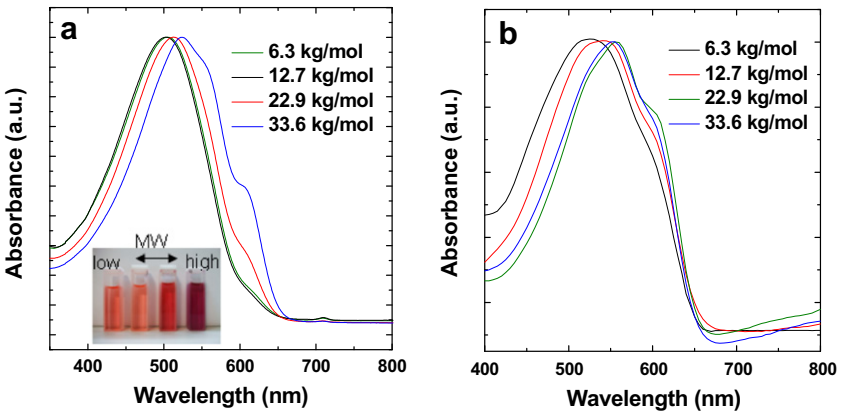

Fig. 1. Optical absorption of Si-PCPDTTBT with various MWs (a) in chlorobenzene solution, and (b) in solid films (spin-coated from chlorobenzene solution). The red-shift of the absorption indicates the larger orbital delocalization by virtue of longer conjugated polymer chains. (Inset: corresponding solution image).

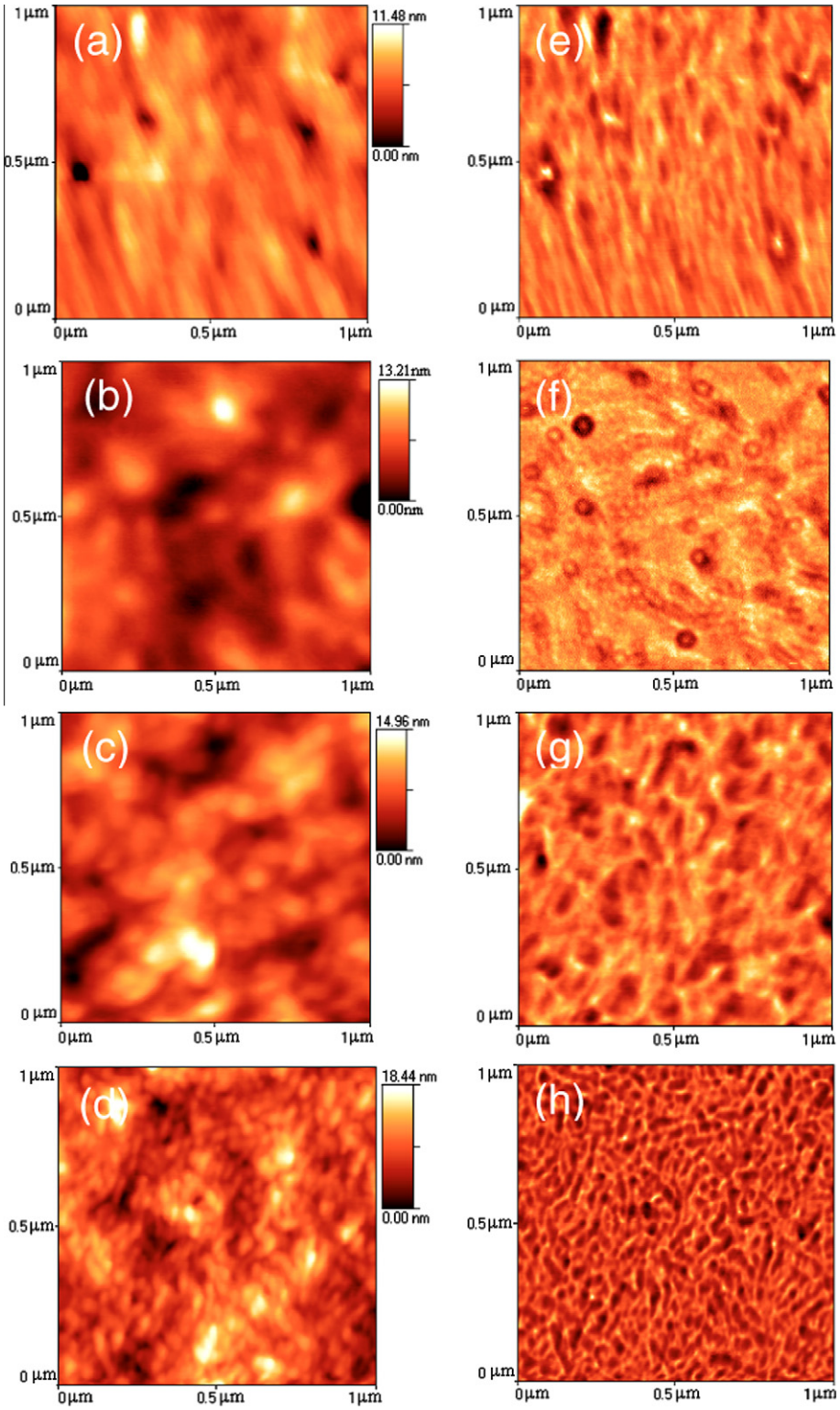

Fig. 2. The AFM images of Si-PCPDTTBT:PCBM films with various MWs for surface morphology (a) 6.3 kg/mol, (b) 12.7 kg/mol, (c) 22.9 kg/mol, (d) 33.6 kg/mol and phase images (e) 6.3 kg/mol, (f) 12.7 kg/mol, (g) 22.9 kg/mol, (h) 33.6 kg/mol.

dialkyl-bithiazole unit and electron-donating thiophene moieties were utilized to synthesize the low bandgap copolymer. Combining with the coplanar siloles, the process of self-organization of polymer into two-dimensional

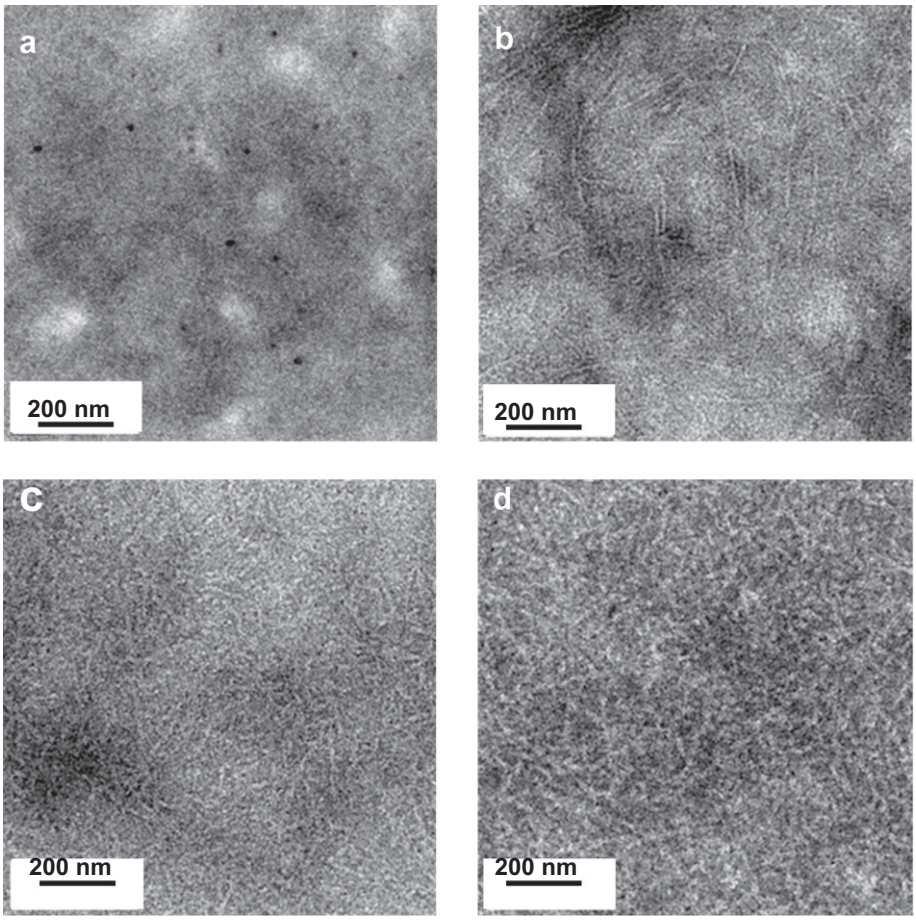

Fig. 3. TEM images of Si-PCPDTTBT:PCBM (1:1) blend films with various MWs. (a) 6.3 kg/mol, (b) 12.7 kg/mol, (c) 22.9 kg/mol, (d) 33.6 kg/mol.

(2D) sheets can be significantly enhanced by means of interchain stacking leading to an enhancement in device efficiency.

Table 1 summarizes the MWs, polydispersities (PDI) and yield of the pristine Si-PCPDTTBT samples used in this study. It should be mentioned that the solubility of Si-PCPDTTBT becomes very poor with MW larger than 33.6 kg/mol (M_n). The thermal stabilities and phase transition temperatures of Si-PCPDTTBT, including 5% weight loss temperatures (T_d), glass transition temperatures (T_g), melting temperatures (T_m), and crystallization temperatures (T_c) characterized by Thermogravimetric analyses (TGA) and differential scanning calorimetry (DSC) are summarized in Table 2. All copolymers are thermally stable up to 375–430 °C upon heating and show T_g values over 163 °C. The T_d and T_g for Si-PCPDTTBT are found to increase with increasing MWs. The increase of thermal stability with higher MW is attributed from stronger π−π interaction and polymer chain entanglement as observed in many polymer systems. In addition, the detectable melting temperatures (T_m) and crystallization temperatures (T_c) of Si-PCPDTTBT suggested that it has great potential in organic solar cells application since their high ordering capabilities can enhance the formation of phase-separated ordered nanostructures in the photovoltaic layer desirable for charge transport and separation.

As shown in the absorption spectra (Fig. 1), with the increase of Si-PCPDTTBT MW, a significant red shift of the absorption for the edge of Si-PCPDTTBT from solution (10^{-6} M in chlorobenzene), together with more pronounced vibronic absorption shoulders is observed. The result indicates that charge carriers and excitons in the higher MW Si-PCPDTTBT can delocalize over a larger extent as a result of π–π stacking and a stronger wave function overlap, and the absorbance band extend from 500 to 525 nm is attributed to a fully delocalized excitonic π–π* transition. The corresponding images for the polymer solution with various MWs are shown in the inset of Fig. 1a. On the other hand, the solid film exhibited an absorption pattern similar to that recorded in solution, except that a slight red-shift occurred in the solid state as a result of interchain association and aggregation. It is worthy to mention that the polymer with higher MWs reveal a pronounced vibronic peak. This indicates that aggregation already occurs for the high MW Si-PCPDTTBT due to the strong π–π interaction in the solution state.

Since morphology has been shown to affect mobility, efforts were made in this study to conduct a comprehensive

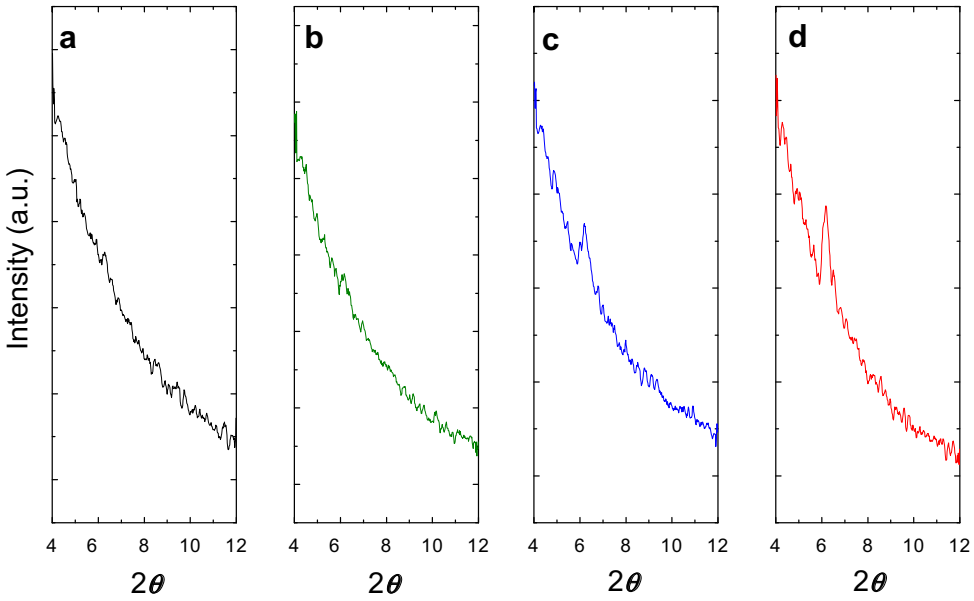

Fig. 4. XRD spectra of Si-PCPDTTBT:PCBM films with various MWs. (a) 6.3 kg/mol, (b) 12.7 kg/mol, (c) 22.9 kg/mol, (d) 33.6 kg/mol.

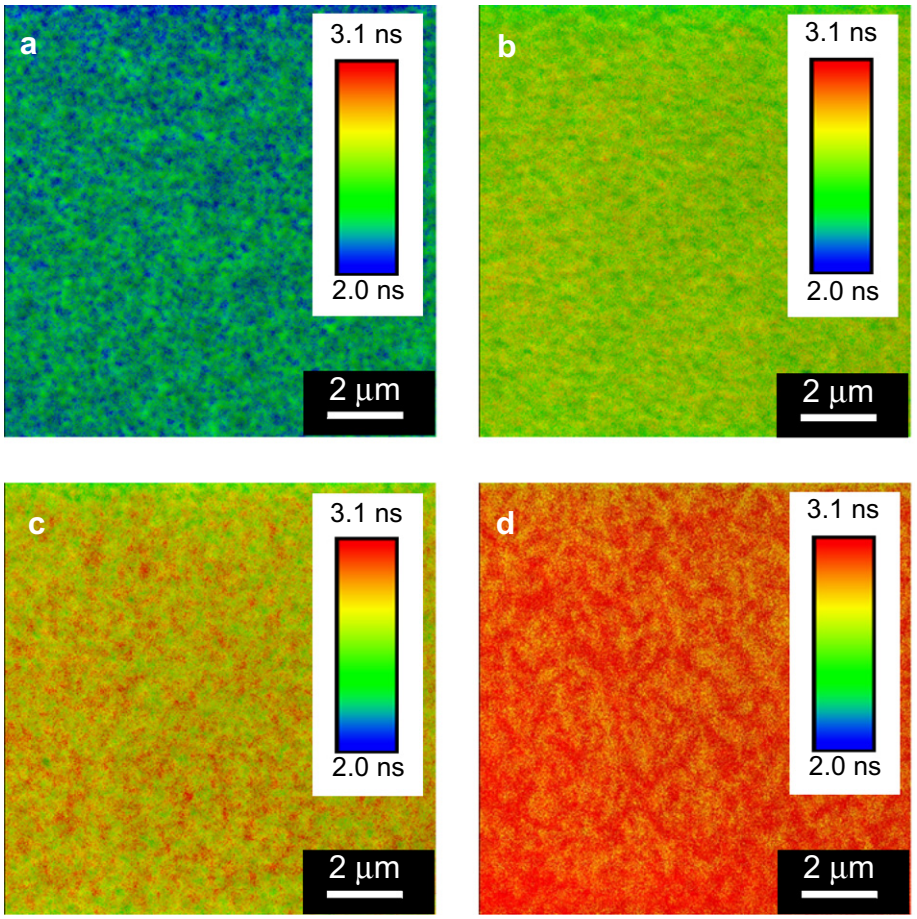

Fig. 5. Exciton lifetime images of the Si-PCPDTTBT:PCBM film with various MWs, (a) 6.3 kg/mol, (b) 12.7 kg/mol, (c) 22.9 kg/mol, (d) 33.6 kg/mol. measured after excitation at 470 nm using a picosecond laser microscope (512 × 512 pixels).

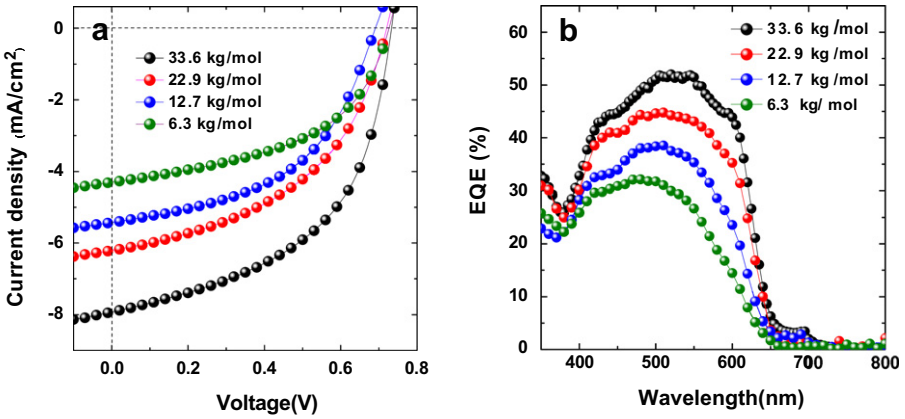

Fig. 6. (a) *J–V* curves and (b) EQE spectra of Si-PCPDTTBT:PCBM-based BHJ solar cells with various MWs.

characterization in terms of MW dependency by AFM and TEM analysis. It has been reported that P3HT with lower MW polymer chains are more able to pack into crystals forming a rod-like morphology [32]. It is interesting; however, the low MW Si-PCPDTTBT reveals very smooth morphology. This can be explained by a much more complicated structure such as Si-PCPDTTBT instead of P3HT, which prevent the polymer chains from stacking. With increasing polymer MW, Si-PCPDTTBT:PCBM films reveal rougher surface morphology with stronger crystallinity. For the 33.6 kg/mol Si-PCPDTTBT/PCBM film, the morphology exhibits coarse, chainlike features, having an average size of 30 nm, running across the surface as shown in Fig. 2d. The corresponding phase images in Fig. 2h also features many channels with a diameter of 20 nm distributed throughout the film originated from the separation between the Si-PCPDTTBT and PCBM. Because the exciton diffusion length in organic materials typically ranges from 10 to 30 nm depending on the mobility, the feature size can offer a certain degree of segregation for the two components to maintain suitable mixing for charge transport and exciton dissociation.

The MW impact on nanoscale morphology is also confirmed by TEM as shown in Fig. 3. In the TEM images, polymer nanofibers look bright and PCBM-rich regions appear dark because of the lower density of polymer crystals compared to PCBM. The TEM images are consistent with the AFM results. For the 6.3 kg/mol Si-PCPDTTBT, hardly any polymer fibers can be discerned. The TEM image of the blending films processed with higher MWs shows phase separation clearly with the appearance of interconnected fibers which are surrounded by darker fullerene-rich regions. With the increase of the polymer MWs, the amount and diameter of Si-PCPDTTBT fibers become larger and coarser. Since the J_{SC} and FF are strongly dependent on the transport properties of the networks in the BHJ film, it can be expected that, at least in part, the formation of the larger domains with wider connective cross sections within the high MW Si-PCPDTTBT network can leads to an improved device performance.

Further investigation of the crystalline nature of Si-PCPDTTBT is accomplished using XRD of polymer films as shown in Fig. 4. The low MW Si-PCPDTTBT exhibits an amorphous pattern indicating the disorder structure. Increased intensity is observed with increasing MW for the peak at $2\theta = 6.17°$, which corresponds to the layering distance, $d_{100} = 14.3$ Å, between the sheets of Si-PCPDTTBT chains associated with the plane perpendicular to their longitudinal axes. The features are in good agreement with the results of AFM and TEM images. It is known that long polymer chains are more prone to entanglement [37]. Hiorns has suggested the entanglement of P3HT may cause the alignment of conjugated segments to be more difficult to achieve, leading to disorder structure [38]. This proposal does not obviously agree with the results displayed here. For the high MW Si-PCPDTTBT, the polymer chains tend to stack and aggregate forming a preferential orientation of the polymer domains. This can be further supported by the charge mobility as shown in Table 3. The charge mobility calculated by space-charge limited current reveals that the holes mobility increases with increasing MW leading to more balanced charge mobility. It is likely that mobility could increase with MW because the closer organization of the polymer chains. Moreover, the charge carriers can travel farther along longer chains before they have to hop to another chain. The net reduction in hopping events could result in an increased mobility. In order to further investigate the optophysical properties of Si-PCPDTTBT/PCBM film with various MWs, we performed the exciton lifetime mapping using time-resolved PL measurement system combining with a confocal laser scanning microscopy [39,40]. This technique enabled us to examine the distribution of the exciton lifetimes within a wide range. Fig. 5 shows the exciton lifetime images (10×10 μm) with the corresponding statistical histograms for these samples. All the samples reveal a uniform exciton lifetime distribution throughout the films. This behavior suggests that good mixing exists between the polymer and the fullerene, leading to a more-efficient energy transfer. The average value of exciton lifetime increases from 2.3 to 3.2 ns with respect to the increase in polymer MW. The slight increase in exciton lifetime can be explained by the better crystallinity of the high MW Si-PCPDTTBT. The enhanced stacking of Si-PCPDTTBT

expels some PCBM molecules from the polymer domain, leading to demixing between the two components which impedes the efficiency of exciton dissociation. Therefore, the average value of exciton lifetime increases with high MW Si-PCPDTTBT.

Fig. 6 presents the current–voltage (J–V) curves and external quantum efficiencies (EQEs) of solar cells incorporating Si-PCPDTTBT blended with PCBM. The V_{OC} remains unchanged at about 0.71 ± 0.02 V even with different MWs of Si-PCPDTTBT. However, the J_{SC} and PCE of the devices vary significantly with polymer MWs as seen from Fig. 6a. The J_{SC} varies from as low as 4.29 mA/cm^2 (for 6.3 kg/mol Si-PCPDTTBT) to as high as 8.7 mA/cm^2 (for 33.6 kg/mol Si-PCPDTTBT). Consistent with the trend in J_{SC}, the EQE magnitude generally increases from 29.3% (6.3 kg/mol Si-PCPDTTBT) to 51.6% (33.6 kg/mol Si-PCPDTTBT). Combining 0.73 V of V_{OC} and 51.9% FF, an efficiency of 3.33% is achieved for the device based on 33.6 kg/mol Si-PCPDTTBT. The correlation between the solar cell performance and the MW of the Si-PCPDTTBT is similar to that of P3HT:PCBM system. The main difference in PCE arises from the better charge mobility and more favorable morphology. For high MW Si-PCPDTTBT, the long polymer chains tend to form the appropriate aggregation in the solution. With such partially aggregated solution, the blending of Si-PCPDTTBT and PCBM can easily produce phase separation during spin coating process to create continuous percolation pathways for charge transport.

4. Conclusion

In conclusion, we have shown the effect of MW on the performance of photovoltaic devices based on Si-PCPDTTBT:PCBM. Morphological analysis indicates that higher MW Si-PCPDTTBT tends to form stacked aggregation and produce better interconnections within the bicontinuous network which can enhance the charge transport. Based on our device performance, the aggregation of Si-PCPDTTBT is an essential process to guarantee high solar cell performance. The PCE can be enhanced from 1.54% to 3.33% for the 6.3 and 33.6 kg/mol Si-PCPDTTBT, respectively. However, the MW of Si-PCPDTTBT cannot be further increased due to the solubility problems. Thus, considering carrier mobility, materials solubility, crystallinity and morphology, the cell performance can be further improved by using mixture of Si-PCPDTTBT with different molecular weights.

Acknowledgements

The authors are grateful to the National Science Council (NSC), Taiwan (NSC 98-2221-E-001-002 and 99-2120-M-009-008-), and Academia Sinica for financial support.

References

[1] G. Yu, J. Gao, J.C. Hummelen, F. Wudl, A.J. Heeger, Science 270 (1995) 1789–1791.
[2] F. Padinger, R.S. Rittberger, N.S. Sariciftci, Adv. Funct. Mater. 13 (2003) 85–88.
[3] H. Kim, M. Shin, Y. Kim, J. Phys, Chem. C 113 (2009) 1620–1623.
[4] Y. Liu, E.N. Mills, R.J. Composto, J. Mater. Chem. 19 (2009) 2704–2709.
[5] S.S. van Bavel, E. Sourty, G. de With, S. Veenstrabd, J. Loos, J. Mater. Chem. 19 (2009) 5388–5393.
[6] J.H. Huang, C.Y. Yang, Z.Y. Ho, D. Kekuda, M.C. Wu, F.C. Chien, P. Chen, C.W. Chu, K.C. Ho, Org. Electron. 10 (2009) 27–33.
[7] H. Tang, G. Lu, L. Li, J. Li, Y. Wang, X. Yang, J. Mater. Chem. 20 (2010) 683–688.
[8] J. Peet, J.Y. Kim, N.E. Coates, W.L. Ma, D. Moses, A.J. Heeger, G.C. Bazan, Nat. Mater. 6 (2007) 497–500.
[9] H.Y. Chen, H. Yang, G. Yang, S. Sista, R. Zadoyan, G. Li, Y. Yang, J. Phys. Chem. C 113 (2009) 7946–7953.
[10] J. Liu, S. Shao, H. Wang, K. Zhao, L. Xue, X. Gao, Z. Xie, Y. Han, Org. Electron. 11 (2010) 775–783.
[11] J.H. Huang, H.Y. Wei, K.C. Huang, C.L. Chen, R.R. Wang, F.C. Chen, K.C. Ho, C.W. Chu, Energy Environ. Sci. 3 (2010) 654–658.
[12] H. Yang, Q. Song, Z. Lu, C. Guo, C. Gong, W. Hu, C.M. Li, Energy Environ. Sci. 3 (2010) 1580–1586.
[13] M. Shin, H. Kim, S. Nam, J. Park, Y. Kim, Energy Environ. Sci. 3 (2010) 1538–1543.
[14] A.W. Hains, C. Ramanan, M.D. Irwin, J. Liu, M.R. Wasielewski, T.J. Marks, A.C.S. Appl, Mater. Interfaces 2 (2010) 175–185.
[15] S.K. Hau, Y.J. Cheng, H.L. Yip, Y. Zhang, P.H. Ma, A.K.Y. Jen, ACS Appl. Mater. Interfaces 2 (2010) 1892–1902.
[16] J.H. Huang, D. Kekuda, C.W. Chu, K.C. Ho, J. Mater. Chem. 19 (2009) 3704–3712.
[17] X. Chen, J. Yang, L.Y.X.C. Haley, J. Lu, F. Zhu, K.P. Loh, Org. Electron. 11 (2010) 1942–1946.
[18] H.W. Tsai, Z. Pei, T.H. Huang, P.W. Li, Y.J. Chan, Org. Electron. 11 (2010) 1796–1801.
[19] P. de Bruyn, D.J.D. Moet, P.W.M. Blom, Org. Electron. 11 (2010) 1419–1422.
[20] G.D. Sharma, P. Suresh, J.A. Mikroyannidis, Org. Electron. 11 (2010) 731–742.
[21] Y.I. Lee, J.H. Youn, M.S. Ryu, J. Kim, H.T. Moon, J. Jang, Org. Electron. 12 (2011) 353–357.
[22] I. Sasajima, S. Uesaka, T. Kuwabara, T. Yamaguchi, K. Takahashi, Org. Electron. 12 (2011) 113–118.
[23] T. Sakurai, T. Ohashi, H. Kitazume, M. Kubota, T. Suemasu, K. Akimoto, Org. Electron. 12 (2011) 966–973.
[24] S. Wang, Z. Bian, X. Xia, C. Huang, Org. Electron. 11 (2010) 1909–1915.
[25] S. Sarkar, J.H. Culp, J.T. Whyland, M. Garvan, V. Misra, Org. Electron. 11 (2010) 1896–1900.
[26] J.H. Kim, J.H. Park, J.H. Lee, J.S. Kim, M. Sim, K. Cho, J. Mater. Chem. 20 (2010) 7398–7405.
[27] C. Müller, E. Wang, L.M. Andersson, K. Tvingstedt, Y. Zhou, M.R. Andersson, O. Inganäs, Adv. Funct. Mater. 20 (2010) 2124–2131.
[28] D.J.D. Moet, M. Lenes, J.D. Kotlarski, S.C. Veenstra, J. Sweelssen, M.M. Koetse, B. de Boer, P.W.M. Blom, Org. Electron. 10 (2009) 1275–1281.
[29] M.C. Wu, C.H. Chang, H.H. Lo, Y.S. Lin, Y.Y. Lin, W.C. Yen, W.F. Su, Y.F. Chen, C.W. Chen, J. Mater. Chem. 18 (2008) 4097–4102.
[30] M.K. Siddiki, J. Li, D. Galipeau, Q. Qiao, Energy Environ. Sci. 3 (2010) 867–883.
[31] W. Ma, J.Y. Kim, K. Lee, A.J. Heeger, Macromol. Rapid Commun. 28 (2007) 1776–1780.
[32] A.M. Ballantyne, L. Chen, J. Dane, T. Hammant, F.M. Braun, M. Heeney, W. Duffy, I. McCulloch, D.D.C. Bradley, J. Nelson, Adv. Funct. Mater. 18 (2008) 2373–2380.
[33] R.J. Kline, M.D. McGehee, E.N. Kadnikova, J. Liu, J.M.J. Fréchet, Adv. Mater. 15 (2003) 1519–1522.
[34] M.C. Scharber, M. Koppe, J. Gao, F. Cordella, M.A. Loi, P. Denk, M. Morana, H.J. Egelhaaf, K. Forberich, G. Dennler, R. Gaudiana, D. Waller, Z. Zhu, X. Shi, C.J. Brabec, Adv. Mater. 21 (2009) 1–4.
[35] H.Y. Chen, J. Hou, A.E. Hayden, H. Yang, K.N. Houk, Y. Yang, Adv. Mater. 22 (2010) 371–375.
[36] J.H. Huang, C.M. Teng, Y.S. Hsiao, F.W. Yen, P. Chen, F.C. Chang, C.W. Chu, J. Phys. Chem. C 115 (2011) 2398–2405.
[37] J.M.G. Cowie, Polymer: Chemistry and Physics of Modern Materials, 2nd. Ed., Blackie Academic & Professional, Glasgow, 1991.
[38] R.C. Hiorns, R. de Bettignies, J. Leroy, S. Bailly, M. Firon, C. Sentein, A. Khoukh, H. Preud'homme, C. Dagron-Lartigau, Adv. Funct. Mater. 16 (2006) 2263–2273.
[39] J.H. Huang, F.C. Chien, P. Chen, K.C. Ho, C.W. Chu, Anal. Chem. 82 (2010) 1669–1673.
[40] J.H. Huang, K.C. Li, F.C. Chien, Y.S. Hsiao, D. Kekuda, P. Chen, H.C. Lin, K.C. Ho, C.W. Chu, J. Phys. Chem. C 114 (2010) 9062–9069.